UNIVERSITATEA “BABEŞ-BOLYAI” CLUJ-NAPOCA

FACULTATEA DE FIZICĂ

SPECIALIZAREA BIOFIZICĂ ȘI FIZICĂ MEDICALĂ

LUCRARE DE DISERTAŢIE

Coordonator științific

Conferențiar Monica Focșan

Absolvent

Dinca Andrei Cristian

2025

UNIVERSITATEA “BABEŞ-BOLYAI” CLUJ-NAPOCA
FACULTATEA DE FIZICĂ
SPECIALIZAREA BIOFIZICĂ ȘI FIZICĂ MEDICALĂ

LUCRARE DE DISERTAŢIE

Gold Nanobipyramids and Nanorods: Synthesis, Plasmonic Sensing, and Photothermal Applications

Coordonator științific
Conferențiar Monica Focșan

Absolvent
Dinca Andrei Cristian

2025

Contents

Abstract

This dissertation investigates the synthesis, functionalization, and application of plasmonic gold nanoparticles (AuNPs) for sensing and photothermal purposes. Gold nanobipyramids (AuBPs) and nanorods (AuNRs) were synthesized via controlled seed mediated approaches, allowing fine-tuning of their localized surface plasmon resonance (LSPR) by adjusting seed concentration and silver nitrate levels. The nanoparticles were subsequently immobilized on i) glass functionalized with a mixture of 5% N-(2-aminoethyl)-3-aminopropylmethyldimethoxysilane and 5% 3-mercaptopropylmethyldimethoxysilane and ii) Polydimethylsiloxane (PDMS) functionalized with (3-Aminopropyl)triethoxysilane (APTES**)** substrates using optimized silanization and surfactant exchange protocols. For the sensing application, the solid plasmonic substrates were tested for lead ion detection via LSPR of AuBPs. The interaction between lead ions and nanoparticle surfaces induced measurable shifts in the extinction spectra of the immobilized AuBPs, enabling detection of lead concentrations as low as 2 μM. These results demonstrate the sensitivity and reproducibility of the system, offering a simple and cost-effective approach for heavy metal detection. Next, the flexible plasmonic substrates coated with either AuBPs or AuNRs were irradiated with lasers and LEDs at various wavelengths (532 nm, 660 nm, 685 nm, and 850 nm). The experiments revealed that the heating efficiency strongly depends on the spectral overlap between the excitation source and the LSPR of the AuNPs. AuBP707 performed best under 532 nm irradiation, AuNR747 under 660–685 nm, and AuBP921 under 850 nm. Additionally, higher nanoparticle coverage, achieved through increased functionalization, led to improved thermal conversion. The results obtained highlight the versatility of gold nanostructures, demonstrating their potential for plasmonic sensing, biomedical photothermal therapy, and broader technological applications that require efficient light-to-heat conversion.

Introduction

The present work aims to investigate the plasmonic properties of gold nanoparticles from two complementary perspectives: their application as LSPR nanosensors for lead ion detection and the evaluation of their efficiency in photothermal conversion processes under irradiation with various light sources. The main objectives of the study were to synthesize gold nanoparticles with well-defined geometries (herein nanobipyramids and nanorods), with tunable localized surface plasmon resonance (LSPR), by controlling synthesis parameters; to functionalize substrates (glass and PDMS) for the efficient immobilization of nanoparticles; to evaluate the sensitivity of plasmonic substrates for the detection of lead ions; and to investigate the photothermal effect of gold nanoparticles under irradiation with laser and LED sources at various wavelengths.

The study focuses on the synthesis and functionalization of plasmonic gold nanostructures, exploring their behavior both in sensing applications and in photothermal processes. The dual functionality of these nanoparticles highlights their versatility and relevance for both analytical and therapeutic applications.

The dissertation is structured as follows:

Chapter 1 provides the theoretical background on AuNPs, and their established applications in sensing and therapy.

Chapter 2 presents the experimental synthesis of gold nanobipyramids, optimization of reaction parameters, functionalization of glass substrates, and their application in lead ion detection.

Chapter 3 focuses on the deposition of gold nanostructures onto flexible PDMS substrates, their irradiation under different light sources, and the evaluation of their photothermal response. The dissertation concludes with a discussion on the experimental results, their implications, and potential applications of the developed plasmonic systems.

The original contributions of this dissertation consist of the controlled synthesis of gold nanobipyramids with tunable LSPR through precise adjustment of seed volume and silver nitrate concentration; the optimization of substrate functionalization protocols to ensure stable nanoparticle immobilization for both sensing and photothermal studies; the demonstration of plasmonic sensing capabilities for lead ions down to 2 μM concentration; and a comprehensive comparative analysis of photothermal performance of different nanoparticle types under multiple irradiation wavelengths.

Chapter 1: Basics of gold nanoparticles and applications

1.1 Introduction to metal nanoparticles

Nanotechnology is a branch of research with hundreds of applications. It refers to the production and utilization of materials at the nanoscale. By convention, materials that are between 1 and 100 nm are considered to be nanomaterials and to be the main instrument in the nanotechnology industry.[1] These nanoparticles are used for a wide variety of purposes, from energy storage in solar and oxide fuel batteries to cosmetics, smart clothes, the food industry, pharmaceutics, medicine, and many others.[2], [3], [4], [5], [6]

Apart from standard nanoparticles, one particular category stands apart due to its special properties—namely, metallic nanoparticles, more specifically, noble metal nanoparticles. Metals, in general, have free electrons (weakly linked), which, when placed in an alternating electric field, undergo collective oscillation (Figure 1.1). These electrons, which are excited by the electric field, are known as plasmons.

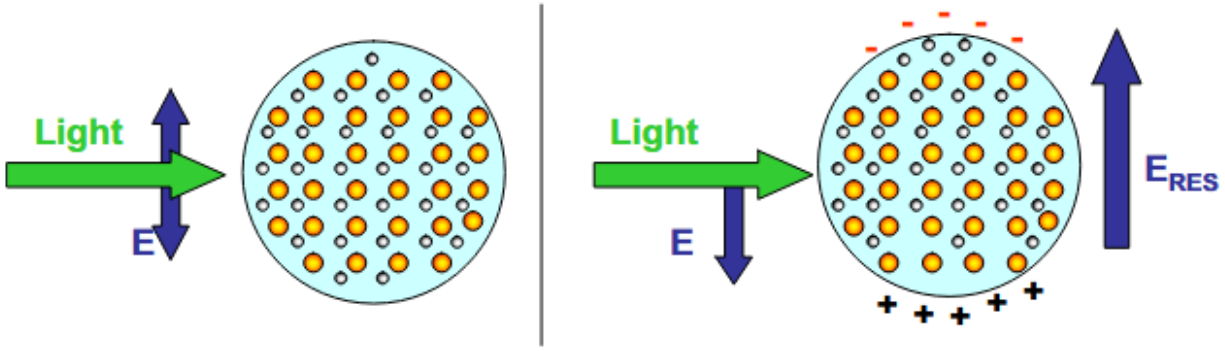

Figure 1.1 – Scheme of the light interaction with a metallic nanoparticle. The external electric field produces a migration of conduction electrons to one side of the nanoparticle, creating an imbalance in the surface charges. This results in the formation of a dipole moment and an electric field opposing the external one.[7]

A cost-effective and accessible method to mesure nanoparticles extinction is via a UV-Vis-NIR spectrophotometer (Appendix 1). This machine measures how much light is allowed to pass through a sample at different wavelengths in the mentioned range. In the case of nanoparticles, it actually measures the extinction cross section (C_{ext}).

$$C_{ext} = C_{Absorbtion} + C_{Scattering}$$

Where: $C_{absorbtion}$ is absorption cross section and $C_{scattering}$ is scattering cross section.

According to Stefan A. Maier[7] :

$$C_{ext} = \frac{4\pi k}{\epsilon_0} \cdot Im(\alpha)$$

Where k is the wavenumer in the medium $k = \frac{2\pi}{\lambda} \cdot n_m$, ε_0 is medium permitivity and α is the polarizability of the particle.

When light hits a nanoparticle, it induces a dipole momentum (p), tipically:

$$p = \alpha E_{inc}$$

E_{inc} is the incident electric field.

$$\alpha = 4\pi\epsilon_0 R^3 \cdot \frac{\epsilon - \epsilon_m}{\epsilon + 2\epsilon_m}$$

Where ε is the dielectric function of the particle and ε_m is the dielectric constant of the surrounding medium.

$$Re[\epsilon(\omega)] = -2\epsilon_m$$

This last equation describes the resonance condition of the sistem were ε(ω) is the dielectric function. This equations covers only the spherical nanoparticles, depending on the shape of the nanoparticles, the light could also create multipole moments resulting in diferent extinction responses. So, of primary importance, is the dipole or multipole moments which are directly corelated with the extinction cross section.

Variations in these parameters result in observable shifts in the extinction spectrum. This underpins one of the primary applications of nanoparticles—their ability to detect environmental changes with high sensitivity, making them excellent candidates for sensor technologies.

1.2 Gold Nanoparticles as sensors

One of the most basic types of sensors made from nanoparticles are those that change color due to aggregation in the presence of the compound of interest. One such example is the detection of alkali and alkaline earth metal ions. Nanoparticles are functionalized with chelating agents. When these complexes come into contact with the specific ions, they aggregate, changing the color of the suspension and thus enabling the detection of the ions at concentrations as low as the millimolar range. As shown in Figure 1.2, nanoparticles functionalized with 15-crown-5 moieties are used for detection of potatassium ions (K^+).[8] By changing the moieties to 12-crown-4, on the nanoparticle surface, sodium ions (Na+) have been detected as well from bodily fluids- specifically, urine.[9] Other ions such as Li^+ and Ca^{2+} have been detected using similar methods, simply by changing the moieties.[10]

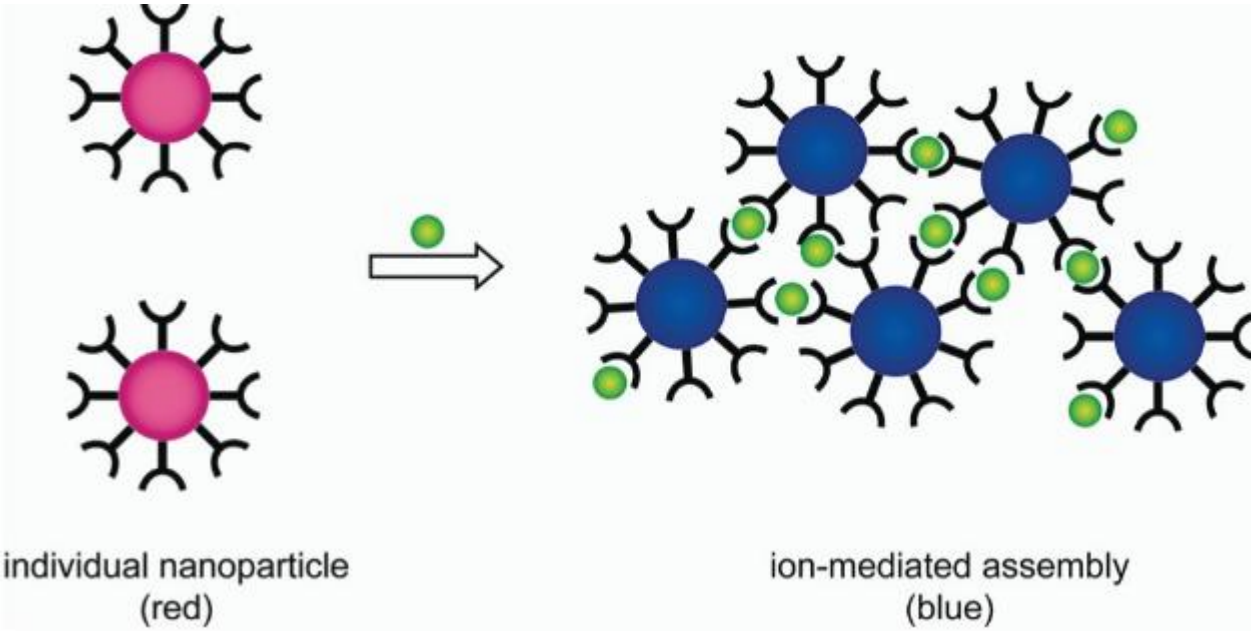

Figure 1.2 Illustrative mechanism of binding between the nanoparticle's moieties and the ions. The color change of the nanoparticle is purely aesthetic, intended to aid in understanding the processes occurring in the nanoparticle suspension. [10]

Similar to alkali metal ions, heavy metal ions can be as well detected by nanoparticle suspensions via simple colorimetric methods e.g. Strouse et al. observed a response for Pb^{2+} ,Cd^{2+} and Hg^{2+} ions at concentration greater than 400 μM.[11]. By imporoving the technique, using the enhanced hyper-Rayleigh Scattering (HRS), the limit range was lowerd to 25 μM. Other studies suggest that by optimizing the buffer solution concentration and layer thickness, one can detect concentrations as low as 100 μM.[12]

Beside metal ions gold nanoparticles can detect small organic molecules (e.g. glucose). Geddes et al. come up with a system of gold nanoparticles coverd with Dextran, this complexes were further functionalized with concanvalin A (Con A). In the presence of glucose Con A breakes the binding with Dextran and creates a bond with glucose (figure 1.3). Further using simple spectroscopic mesurements such as Uv-Vis spectrometry can mesure simple dextran functionalized gold nanoparticles and in doing so detect how much of Con A has been relesed, subsequently being able to mesure the glucose concentrations up to mM. This method proves to be usefull to both diabetic (2-40mM) and not-diabetic (3-8mM) pacients.[13]

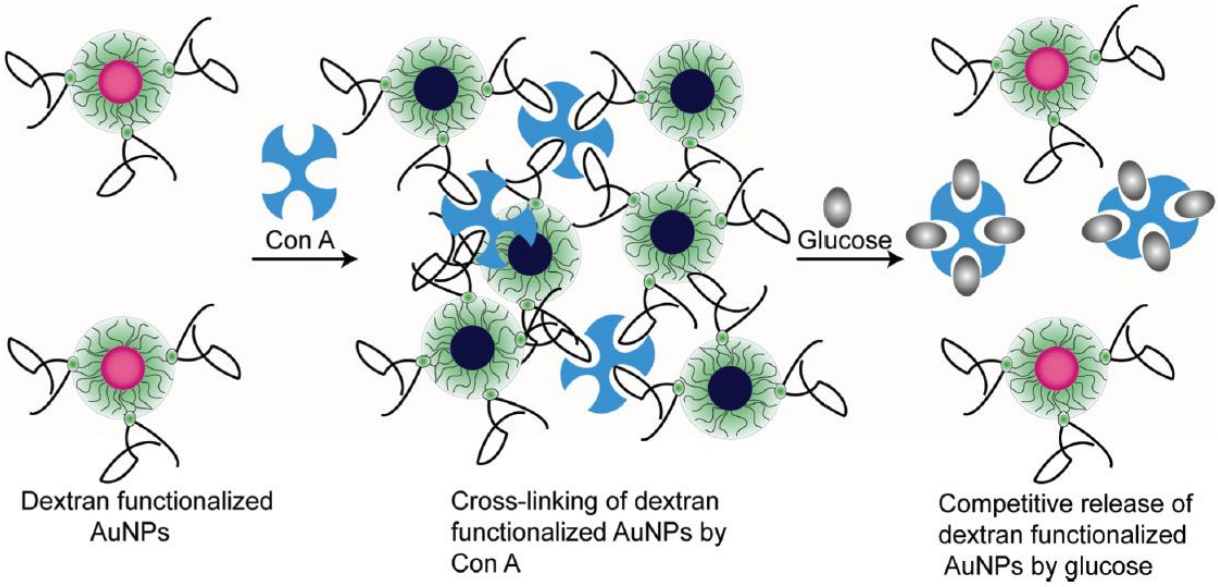

Figure 1.3 Dextran functionalized nanoparticle were added Con A, and the release of Con A in the presence of glucose[10]

As has been shown, gold nanoparticles can be functionalized with a diverse palette of molecules to detect highly specific biomarkers for diagnostic purposes in biomedical applications. According to the World Health Organization, disability and death due to Parkinson's disease (PD) are rapidly increasing. PD currently has no cure, but treatments exist that help patients slow the progression of the disease. However, the main issue is that diagnosis typically occurs at a late stage, when symptoms are already present.

Recent techniques, such as the seed amplification assay (SAA), show promise for early detection [14], but these methods are expensive and not widely accessible. PD is usually associated with a deficiency in dopaminergic neurons in the substantia nigra region of the brain, leading to low dopamine levels and improper sensing of brain stimuli. One potential method for early detection of PD is monitoring dopamine levels. For such applications, gold nanoparticle complexes may offer a viable solution. Su et al. demonstrated the detection capabilities of gold nanoparticles, achieving a detection limit as low as 0.1 μM.

As shown in Figure 1.4, after the reduction of gold salt, dopamine is added to the solution, followed by copper ions and $NaClO_4$. This causes the gold nanoparticles to aggregate around the copper ions. The color of the solution changes from wine red to blue, and detection can be done either by the naked eye or more precisely using a UV-Vis spectrophotometer.[15]

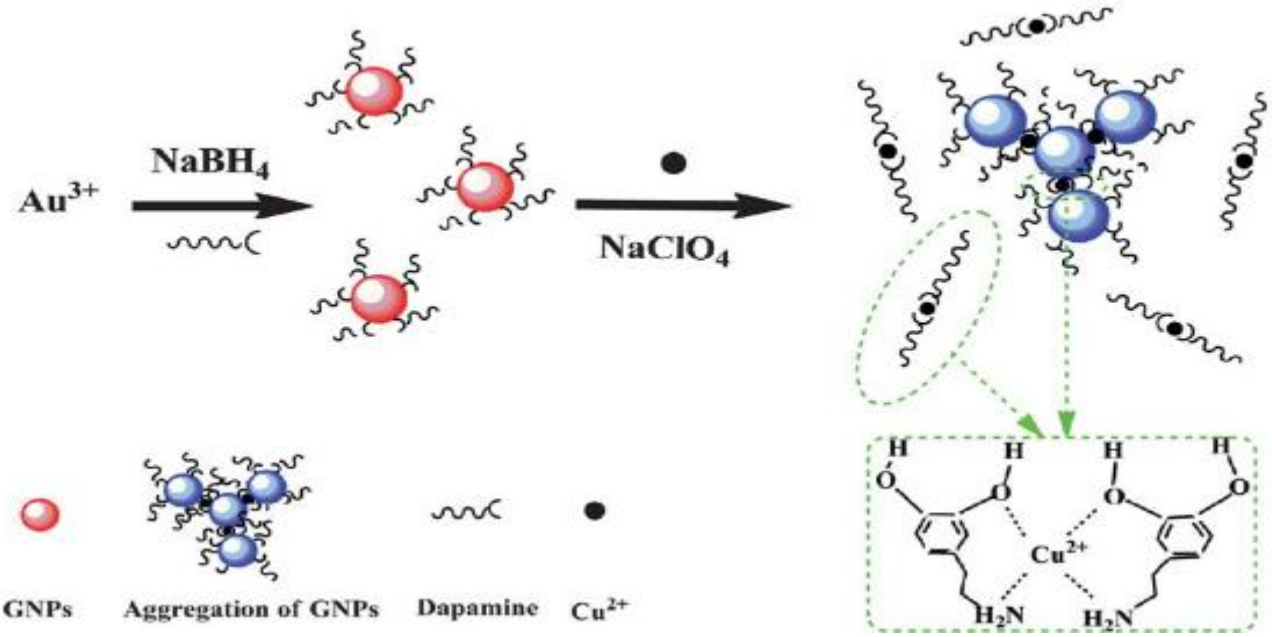

Figure 1.4 Ilustrative mechanism of dopamine sensor [15]

1.3 Nanoparticles used for therapy

Gold nanoparticles are primarily employed in the literature for therapeutic purposes in two major contexts: photodynamic therapy (PDT) and photothermal therapy (PTT), both commonly used in cancer treatment. PDT involves the use of a photosensitizer (PS), which is typically conjugated to a nanoparticle and functionalized to specifically target tumor cells.

Upon irradiation of the tumor site containing the PS, the system undergoes electronic excitation—an electron is promoted to a higher-energy molecular orbital. From this excited state, the system can return to the ground state via three primary pathways: fluorescence, internal conversion (resulting in heat generation), and intersystem crossing. The latter leads to a more stable triplet state due to spin inversion and is characterized by a longer lifetime.

In this triplet state, the system has sufficient time to transfer energy to molecular oxygen, leading to the formation of reactive oxygen species (ROS). These ROS induce oxidative stress, ultimately resulting in cellular damage and death.(figure 1.5)

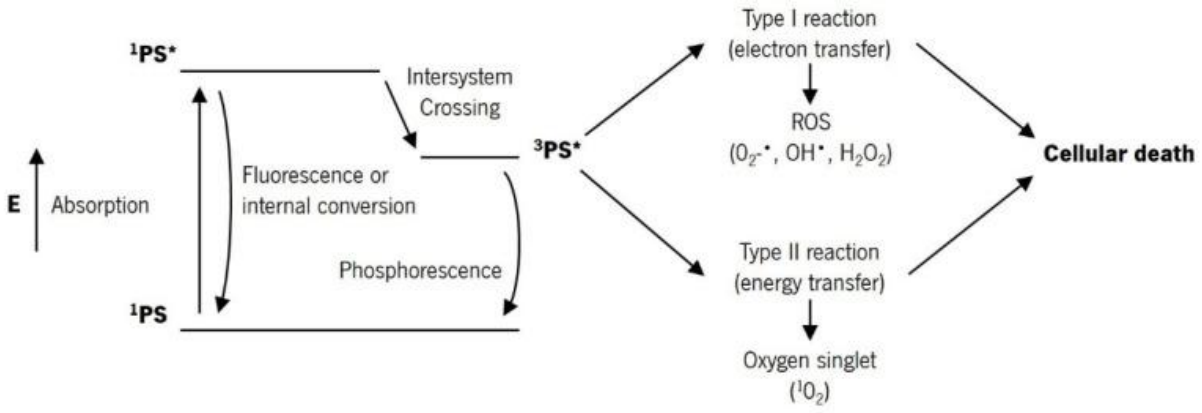

Figure 1.5 Explanatory diagram of photosensitizer energy levels after light excitaion[16]

PTT, on the other hand, focuses on the light-to-heat conversion efficiency of gold nanoparticles. When a photon interacts with a nanoparticle, it excites plasmons. Depending on the nanoparticle's material and size, a portion of the photon's energy is converted into heat. This non-equilibrium heating rapidly increases the nanoparticle's surface temperature through electron–electron scattering. Subsequently, a 'waterfall' phenomenon occurs: the nanoparticle begins to cool via electron–phonon and phonon–phonon coupling, resulting in the dissipation of the heat into nearby medium.[17](figure 1.6)

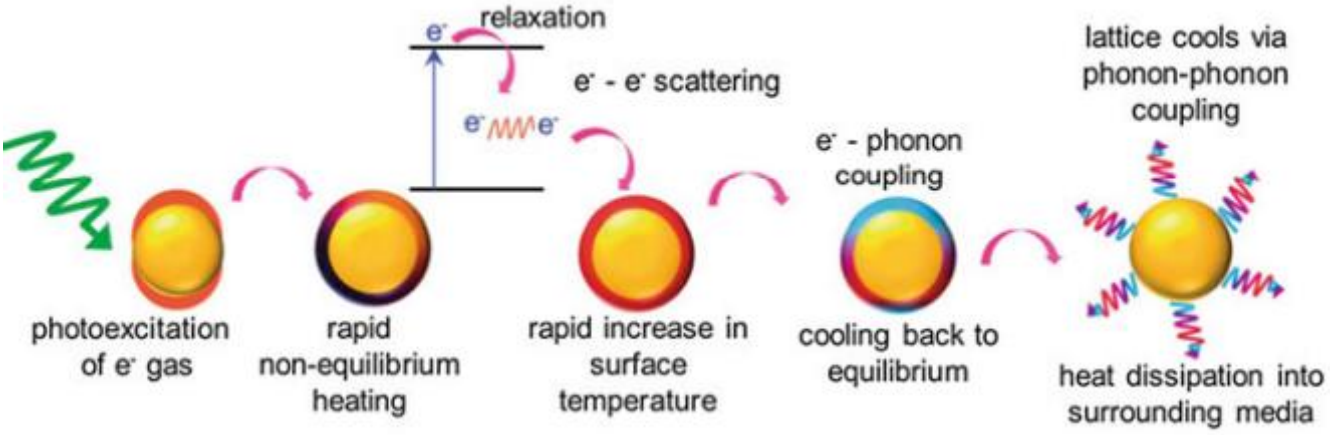

Figure 1.6 The procces of nanoparticle of generating heat when interacting with photons of specific wavelength[17]

Moreover, to maximize the efficiency of photothermal therapy (PTT), near-infrared (NIR) light is used to ensure greater tissue penetration, and nanoparticles are functionalized to also deliver drugs. Adnan et al. studied the effect of different nanoparticle shapes (spheres, rods, and stars — see Transmission Electron Microscopy images in Figure 1.7) in PTT and their ability to deliver drugs (e.g., doxorubicin in this study). The results indicate that, in terms of drug delivery, although spherical nanoparticles achieved the highest grafting density of the drug-conjugated polymer, they were less effective in releasing it compared to star-shaped nanoparticles. The latter demonstrated rapid accumulation of doxorubicin in the

nuclei of cancer cells, indicating effective drug release at the target site. The photothermal effect was measured using a consistent nanoparticle concentration of 125 µg/mL. The most promising results came from gold nanorods, which heated up to 70 °C, followed by nanostars at 62 °C, and spherical nanoparticles at 53 °C.[18]

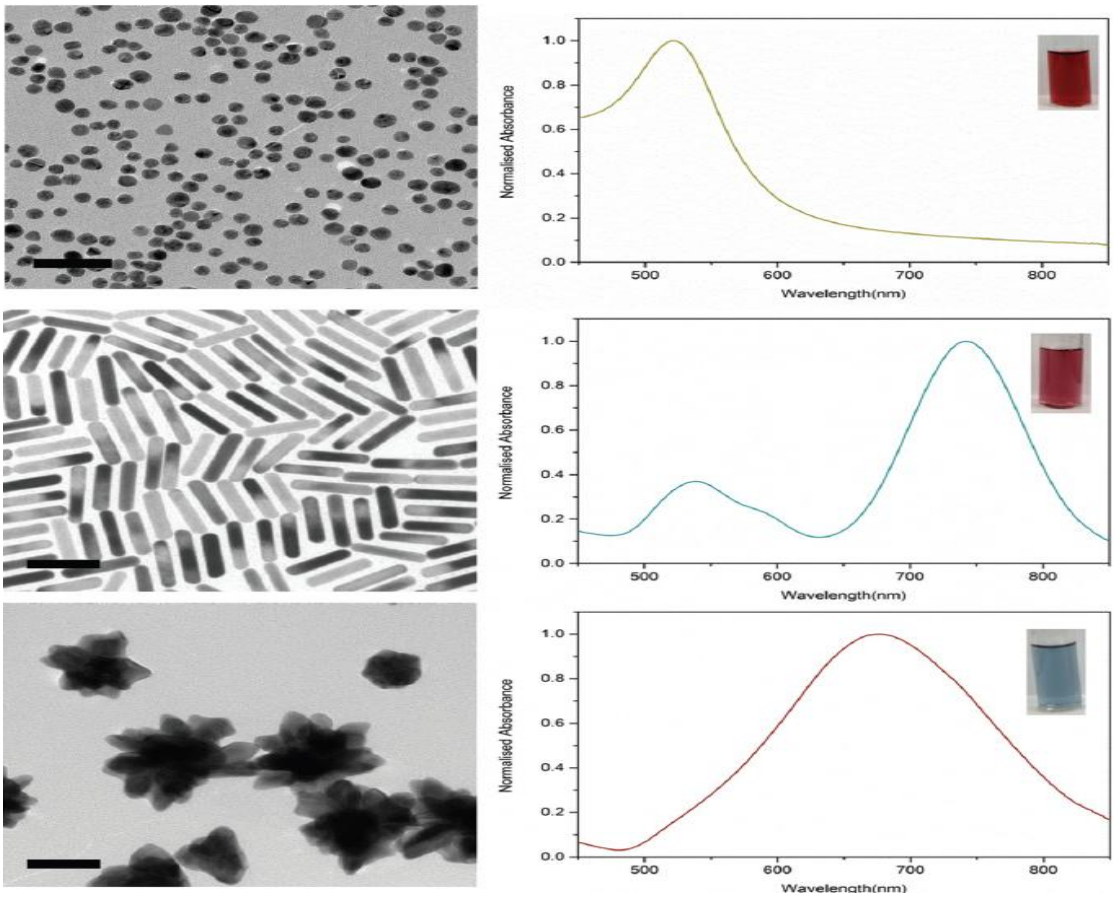

Figure 1.7 Left: TEM images of different gold nanoparticles 50µm scale and their normalized extinction spectra right[18]

Another study approached the problem theoretically and simulated three different nanoparticle shapes: rods, shells, and prisms. Donghyuk et al. modeled these nanoparticles to identify the optimal shape for maximizing efficiency while minimizing thermal damage to the surrounding tissue. They found that nanorods with a length of 28 nm and a diameter of 8 nm were the most effective.[19] Florez et al. studied the difference between spheric nanoparticle and anisotropic naoparticles of sized between 15 and 20nm. They concluded that in this case the anisotropical nanoparticles performed better, reducing cell vibility down to 60% at a concentration of 100 µM.[20]

It appears that gold nanorods are the best candidates for photothermal therapy, but there is still room for improvement in achieving the optimal local effect without damaging the surrounding tissue. In their study, Diez et al. compared commercial gold nanorods (CGNRs) with large and small gold nanorods (LGNRs and SGNRs) in terms of photothermal efficiency. They concluded that small and commercial

gold nanorods exhibit similar conversion yields, while long gold nanorods offer a better option regardless of the concentration used, as shown in Table 1.1. The LGNRs had an average length of 68 ± 4 nm and an average diameter of 20 ± 2 nm.[21]

Concentration (μg/mL)	Temperature Increment (°C)		
	CGNRs	SGNRs	LGNRs
10	17.5	17.7	25.6
5	12.0	9.8	18.9
2	7.3	8.7	14.5
1	7.2	5.5	10.7

Table 1.1 The temperature increment based on naoparticle's size and their concentrations [21]

Chapter 2: Gold nanobipyramids as a lead sensor

2.1 Controlled synthesis of gold bipyramids of different sizes

One method for producing gold nanobipyramids is wet chemical synthesis. This approach involves mixing a seed solution with a growth solution. To obtain nanostructures with sharp tips (nanobipyramids or nanojavelins), the seed particles must be multiply twinned particles (MTPs), often with pentagonal twinning, as these serve as the structural basis for the growth of bipyramidal nanoparticles.

The seed synthesis typically involves combining gold salt ($HAuCl_4$, chloroauric acid) with a strong reducing agent ($NaBH_4$, sodium borohydride) in the presence of a surfactant (CTAC, cetyltrimethylammonium chloride). Although the reaction can be performed at room temperature, the reducing agent ($NaBH_4$, sodium borohydride) must be kept at 4 °C until use to maintain its stability and reactivity.[22]

Apart from the concentration of each chemical, a critical parameter in this step is the rate of addition of the reducing agent and the stirring speed (RPM). Variations in any of these parameters can lead to the formation of seeds of different sizes, which in turn affect the final size and shape of the nanobipyramids.[23] Figure 2.1 shows the extinction spectra of two samples of gold nanobipyramids, obtained via seed mediated approach using different seeds.We named them RS (red seeds) and BS (blue seeds). It can be observed that the extinction peaks differ, indicating that the nanostructures have different sizes, even though the growth solution was identical for both samples. This variability makes it difficult to achieve reproducibility between syntheses. In practice, scientists produce large quantities of a single type of seed and optimize the synthesis conditions based on those seeds. This approach allows for better control over the nanoparticle shape and its corresponding extinction peak.

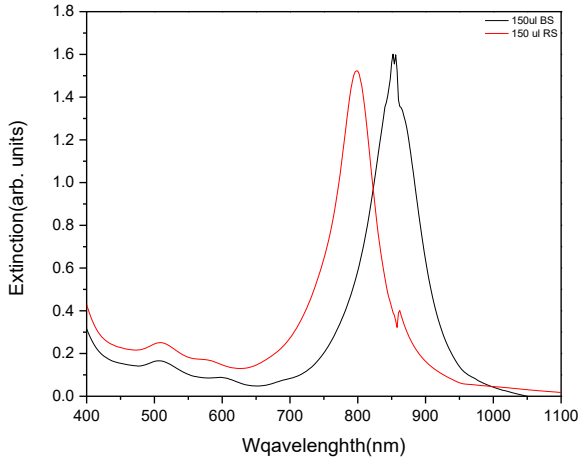

Figure 2.1 Extinction spectra of two nanobipyramids samples using different seeds red:RS, dark:BS

The growth solution is composed of a surfactant (CTAB, cetyltrimethylammonium bromide, 16.5 g/L), $HAuCl_4$ (0.272 g/L), $AgNO_3$ (silver nitrate, 0.85 g/L), a reducing agent (HQL, hydroquinone), and seeds. I used the following volumes for my growth solution: 4 mL CTAB, 40 µL $HAuCl_4$, 30 µL $AgNO_3$, 50 µL hydroquinone, and 150 µL seeds. The reaction takes place at room temperature. First, CTAB is added to a flask, followed by the gold and silver reagents. Then, the reducing agent is added, and the solution is mixed thoroughly until it becomes transparent. Finally, the seeds are added, and the solution is kept at 45°C for 45 to 60 minutes. After each step, the mixture is checked for clarity; if the solution remains cloudy despite thorough mixing, it indicates that one of the reagents may no longer be viable.

Assuming the same growth solution, the only variable being the amount of seed solution added, the gold ions in the mixture are distributed among all the seeds. Therefore, a larger volume of seeds will result in the formation of more nanoparticles, but each individual nanoparticle will be smaller compared to those produced with a lower seed volume.

An easy way to evaluate this effect is by comparing two such samples (Figure 2.2). The localized surface plasmon resonance (LSPR) arises from the longitudinal oscillation of conduction electrons. As the size of the nanoparticles increases, the energy of the associated LSPR peak decreases (i.e., the peak shifts to longer wavelengths). Consequently, a higher seed volume produces more nanoparticles with a lower average size, leading to an LSPR peak at shorter wavelengths but with higher intensity.

This interpretation is supported by SEM images. The results, summarized in Table 2.1, show that using 300 µL of seed solution yields smaller nanoparticles in diameter (75±3 nm) compared to using 150 µL of seeds (102±4 nm).

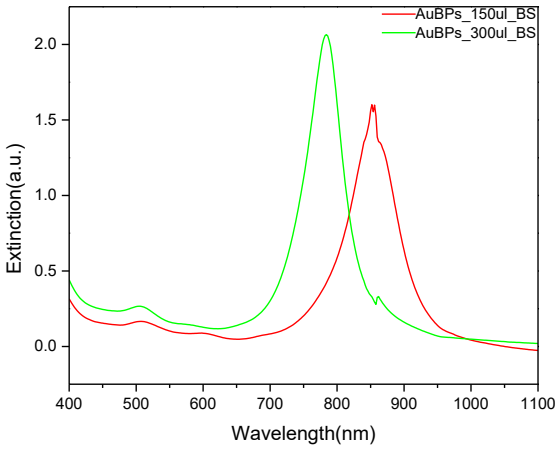

Figure 2.2 Extinction spectrum of AuBPs synthesised with 150 µL of seed red line, 300 µL of seeds green line

Another parameter that can affect the synthesis is the concentration of silver nitrate. As reported by Chateau et al., lowering the silver nitrate concentration tends to cause truncation of the tips of the gold

nanoparticles. Conversely, increasing the concentration results in sharper nanoparticle tips. These morphological changes directly impact the localized surface plasmon resonance (LSPR).[23]

Figure 2.3 illustrates the effect of varying silver nitrate concentration on two different seed solutions. Normally, an increase in silver nitrate leads to the formation of sharper nanoparticles, which enhances local electric field and results in a redshifted LSPR peak with higher intensity compared to samples with lower silver nitrate content.

However, in the case of the samples shown in Figure 2.3, it appears that the silver nitrate was added in excess (10 µL was too much). This likely led to uncontrolled deposition and the formation of silver shells around the gold nanoparticles, which in turn reduced the LSPR signal intensity.

The discrepancies observed in the spectra at 850 nm are attributed to a change in the detection system of the apparatus, and not to differences in the nanoparticle samples themselves.

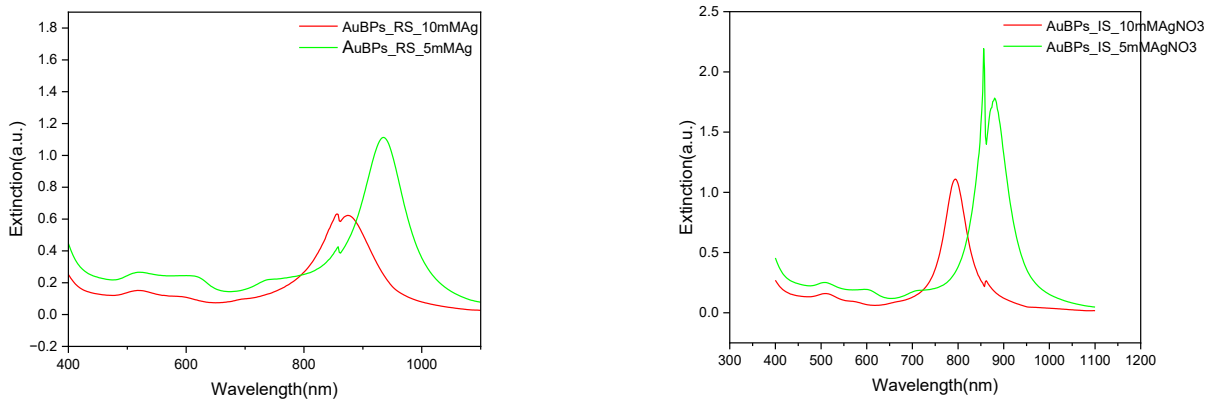

Fugure 2.3 Left: Extinction spectra of AuBPs synthesized using RS with 10 µL (red) and 5 µL (green) of silver nitrate. Right: Corresponding spectra for AuBPs synthesized with Indigo seeds under the same silver nitrate conditions.

Next, with the aim of synthesizing gold nanobipyramids approximately 100 nm in length and exhibiting a localized surface plasmon resonance (LSPR) at 800 nm, I attempted to optimize the synthesis parameters accordingly. I used four types of seed solutions, referred to as balloon seeds, blue seeds (BS), red seeds (RS), and indigo seeds (IS). After nanoparticle synthesis, extinction spectra were recorded, followed by scanning electron microscopy (SEM ;see Appendix 2) imaging (Figure 2.4). The results are summarized in Table 2.1.

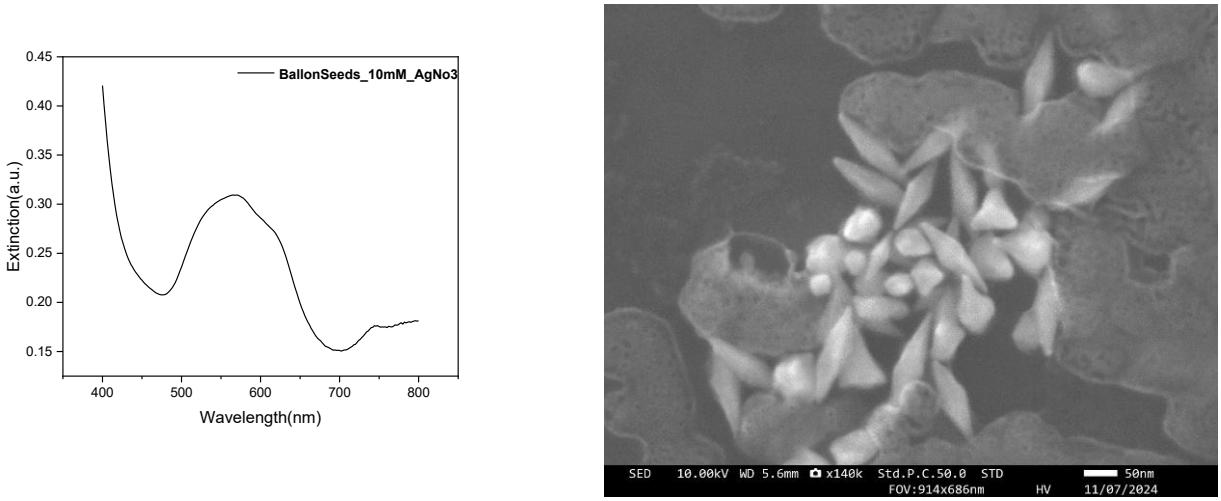

Figure 2.4 Left extinction spectrum of AuBPs synthesized with ballon seeds and right their coresponding SEM image

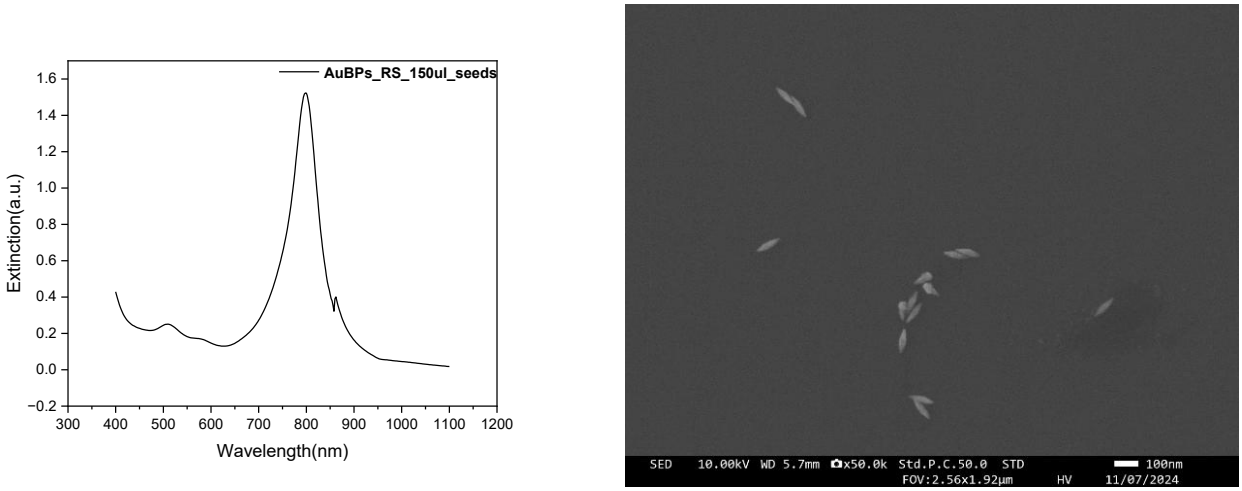

Figure 2.5 Left extinction spectrum of AuBPs synthesized with 150 µL of RS and right their coresponding SEM image

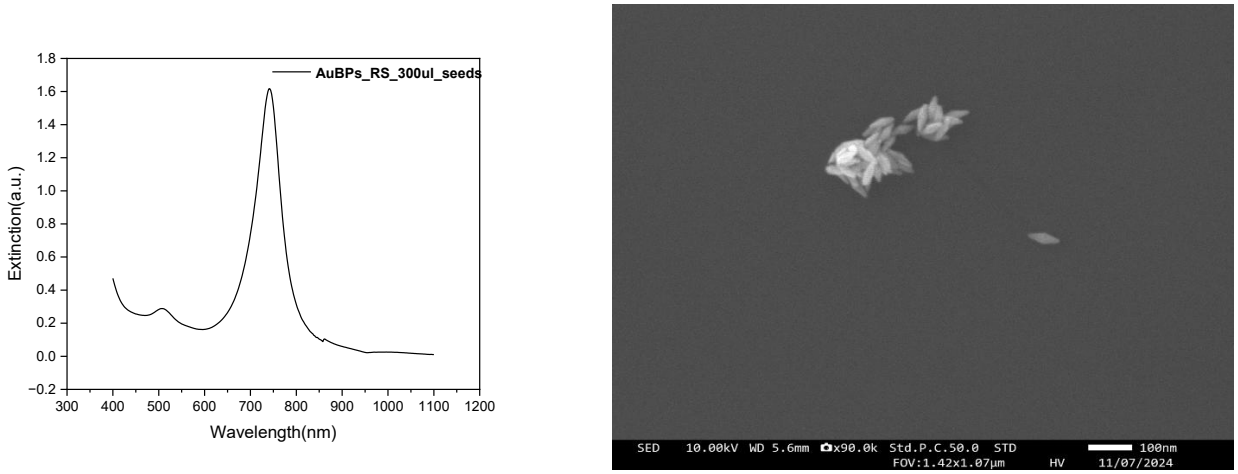

Figure 2.6 Left extinction spectrum of AuBPs synthesized with 300 µL of RS and right their coresponding SEM image

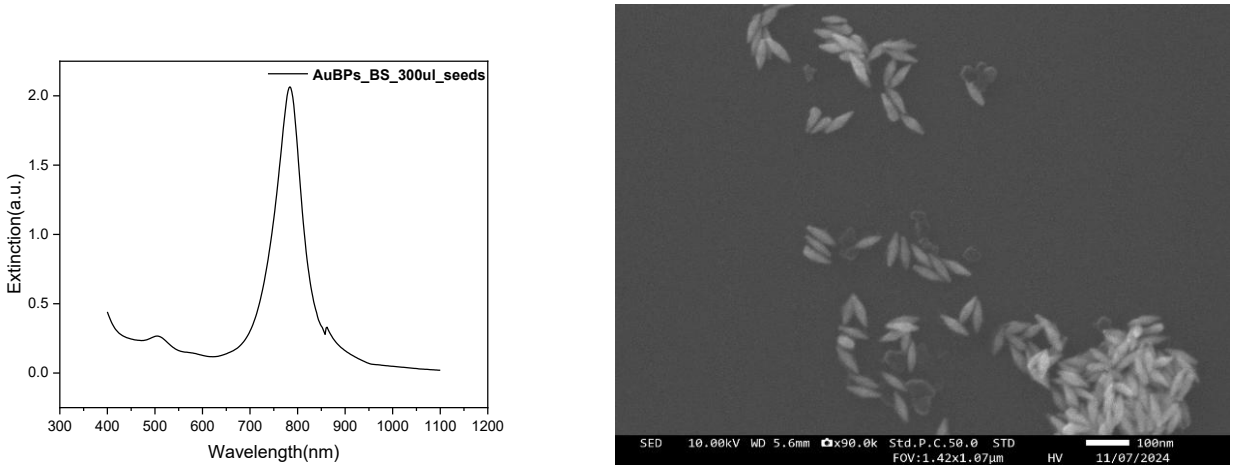

Figure 2.7 Left extinction spectrum of AuBPs synthesized with 300 µL of BS and right their coresponding SEM image

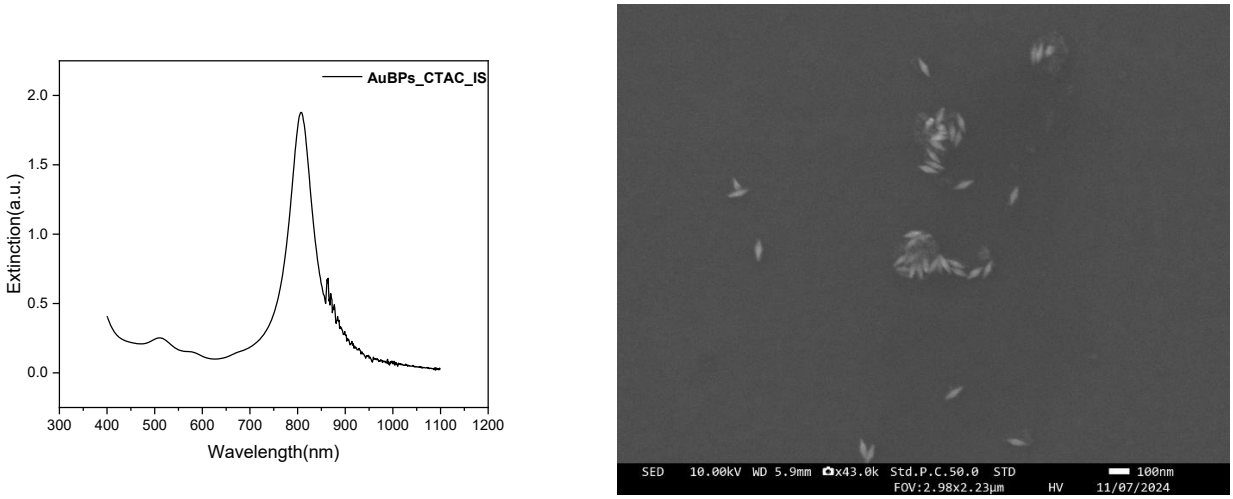

Figure 2.8 Left extinction spectrum of AuBPs synthesized with 40 µL of IS and right their coresponding SEM image

Seeds	Length(nm)	LSPR
Ballon 40ul	143±8	Not a band
Blue 150ul	102±4	852nm
Blue 300ul	75±3	782nm
Red 300ul	67±4	739nm
Indigo 40ul	101±5	808nm

Table 2.1 Summarized results of images 2.4 through 2.8. The length refers to AuBPs diameters from the SEM images and their wavelength coresponding LSPR band

2.2 Cleaning protocol and deposition on glass

For substrate deposition, a glass slide coated on one side with indium tin oxide (ITO) was used. The ITO-coated glass was sonicated at 40 °C for 1.5 hours in a sequence of cleaning steps: 15 minutes in a 50% solution of a laboratory-grade detergent (DFT4), followed by two rinses in ultrapure water for 15 minutes each, two rinses in acetone for 15 minutes each, and finally 15 minutes in methanol. After the chemical cleaning was completed, the substrate was immersed for 1h in a 10% silane solution to silanize the surface (Figure 2.9). Silanization is an important step because it enables the chemical binding of gold nanoparticles to the glass surface.[24] The silanized substrate was further cleaned to remove excess silane by sonicating it in methanol for 15 minutes. Afterward, the methanol was removed, and the substrate was dried at 120 °C for 30 minutes. The silane solution used for surface functionalization consisted of a mixture of 5% N-(2-aminoethyl)-3-aminopropylmethyldimethoxysilane and 5% 3-mercaptopropylmethyldimethoxysilane.

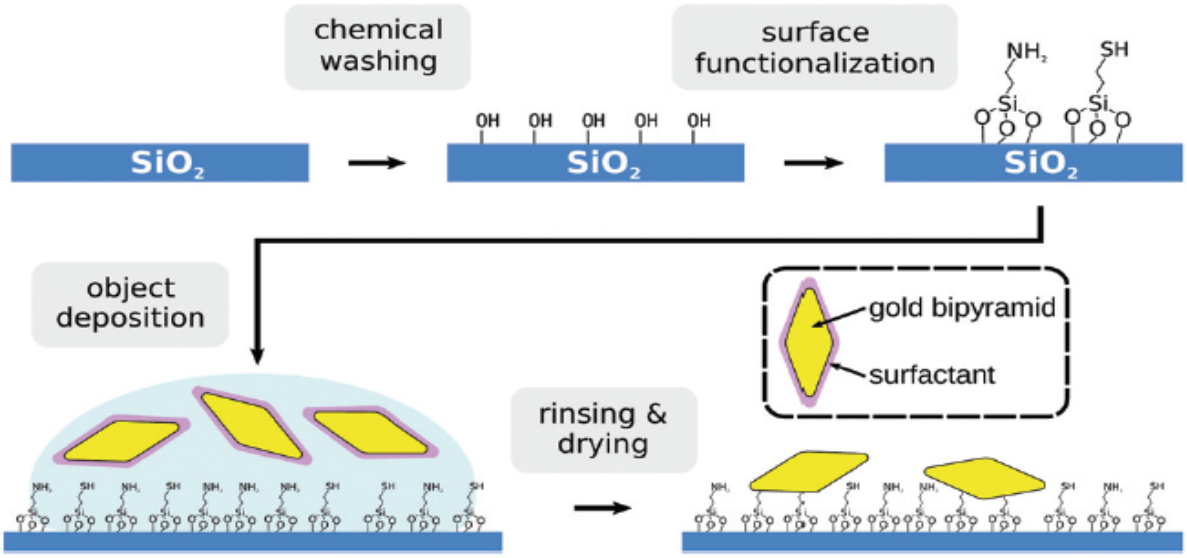

Fiugre 2.9 Schematic illustration of the grafting process of gold nanoparticles onto a silanized glass substrate.[24]

When we tried to bind CTAB covered nanoparticles to the glass substrate we fould that very little amount of nanoparticles were sticking to the substrate (figure 2.10).

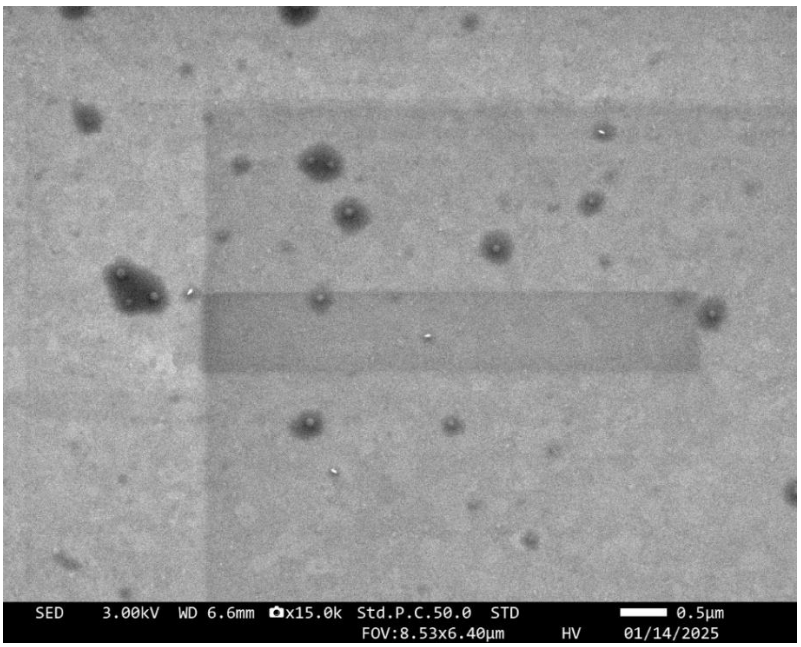

Figure 2.10 SEM image of CTAB covered gold bipyramids on glass substrate

In order to overcome this hurdle, we replaced the surfactant on the surface of the nanoparticles using the method described by Mathala et al., in which CTAB is first exchanged with poly(sodium 4-styrenesulfonate) (PSS), and then with citrate.[25]

Citrate, being a more reactive surfactant, bound more efficiently to the functionalized surface (Figure 2.11), allowing the extinction spectra of the immobilized nanoparticles to be recorded on the substrate (Figure 2.12).

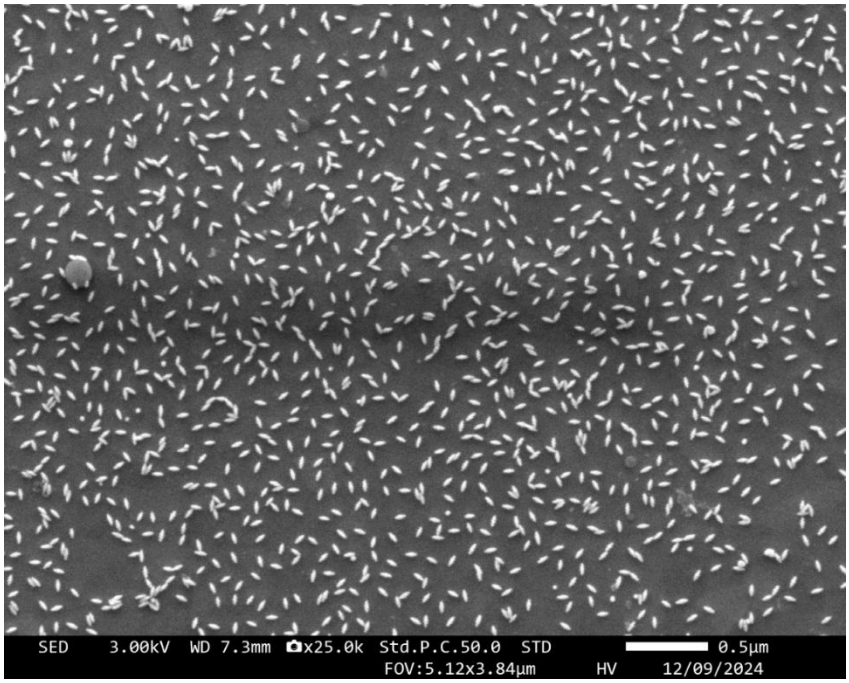

Figure 2.11 SEM image of the citrate covered gold nanobipyramids on glass substrate.

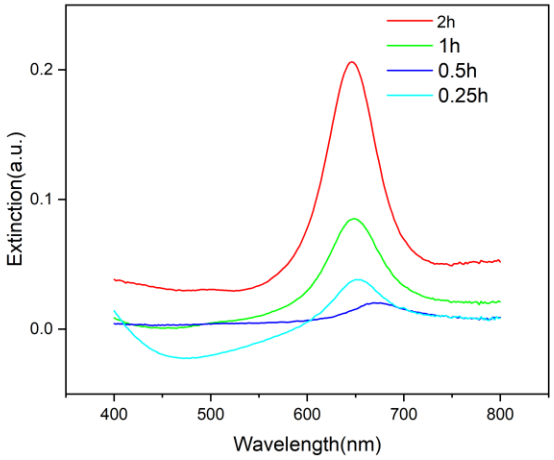

Figure 2.12 Extinction spectra of citrate covered gold nanobipyramids on glass functionalized substrate with different imersion time

2.3 Lead sensing

After the solid plasmonic substrate was confirmed to be reproducible, it was exposed to lead ions using a lead nitrate ($Pb(NO_3)_2$) solution. A 5 mM concentration of lead nitrate was prepared, and the substrate was immersed for 5, 10, 15, 20 minutes, and so on. After each immersion, an extinction spectrum was recorded. It was observed that the intensity of the localized surface plasmon resonance (LSPR) peak decreased. This decrease can be attributed to the loss of nanoparticles with each immersion, as well as the deposition of lead ions on the nanoparticle surfaces (Figure 2.13), which also explains the red shift observed (Figure 2.14) after approximately 20 minutes of immersion at the 5 mM concentration.

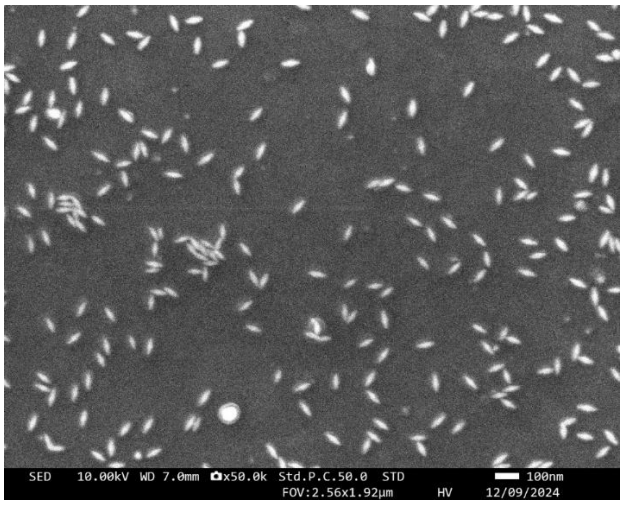

Figure 2.13 SEM image of 50 min immersion time of plasmonic glass substrate in lead nitrate 5mM

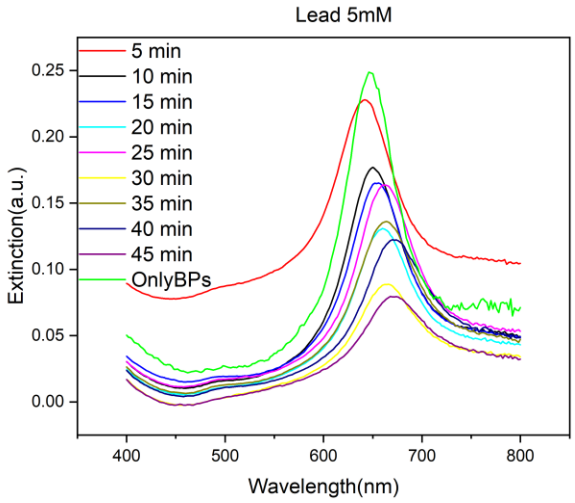

Figure 2.14 Extinction spectra of the solid plasmonic substrate exposed to lead nitrate 5mM for different amounts of time

Next the substrates were immersed in lower concentration of lead nitrate. The last concentration where lead could still be observed was 2 μM. (Figure 2.15) Multiple lower concentration were tried, but no response was registered, this setting the ability of his complex to detect lead to 2 μM.

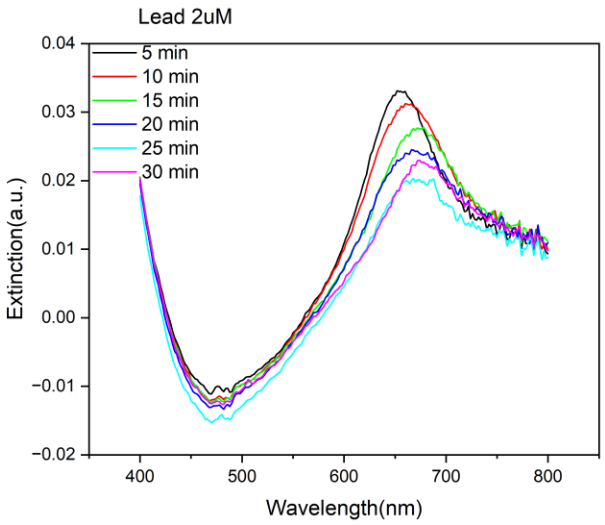

Figure 2.15 Extinction spectra of plasmonic substrate exposed to lead nitrate 2μM for different amounts of time

The synthesis and characterization of gold nanobipyramids demonstrated the critical influence of seed type and reaction parameters on nanoparticle size, morphology, and plasmonic properties. By carefully adjusting seed volume and silver nitrate concentration, bipyramids with distinct LSPR peaks ranging from 739 nm to 852 nm were successfully produced. Functionalization of glass substrates with silane chemistry, combined with surfactant exchange protocols, enabled stable nanoparticle immobilization suitable for sensing applications. The lead detection experiments confirmed that the plasmonic substrates exhibit sensitivity down to 2 μM Pb^{2+}, with observable LSPR red shifts and extinction decreases upon ion binding. These results highlight the potential of gold nanobipyramids as reliable plasmonic sensors for detecting heavy metal ions in aqueous environments, combining both high sensitivity and simple detection protocols.

Chapter 3: Phototermal effect of gold bipyramids and nanorods on flexible substrate

3.1 Flexible PDMS (polydimethylsiloxan) substrate fabrication and functionalization

In the first part of this dissertation, glass was chosen as the material because SMS (spatial modulation spectroscopy)—a technique that can further lower the detectable concentration—does not support other substrates. This method will be used to further improve the sensor developed in the initial stage of the study. However, for the next part of the study, it was considered more useful to use a material that is transparent, flexible, and non-brittle to facilitate transport under various conditions and enhance versatility. One such material is PDMS.

For the synthesis of PDMS, an elastomer and a curing agent were used in a mass ratio of 10:1. After both components were added to the same container, the mixture was stirred thoroughly until it became homogeneous. The next step involved subjecting the mixture to a mild vacuum for 30 minutes to remove gases (air) from the composition. Following this procedure, the mixture underwent thermal treatment for one hour at a temperature of 65 °C. For efficiency reasons, one large batch was made and then cut into smaller circles so that multiple substrates could be tested individually (figure 3.1).

Figure 3.1 Image of transparent and flexible PDMS substrate that was used in this chapter

PDMS layers were subjected to an ethanol cleaning for 5 minutes, followed by a 20-minute ozone treatment. The substrates were then immersed for 1 hour in either 3% or 5% APTES((3-Aminopropyl)triethoxysilane). After this process, the substrates with linker molecules were immersed

for 1 hour in a gold colloidal suspension containing either nanobipyramids (AuBP+LSPR) or nanorods (AuNR+LSPR), their extinction spectra can be observed in figure 3.2. The substrates were called :AuNR746, AuBP922 and AuBP707.

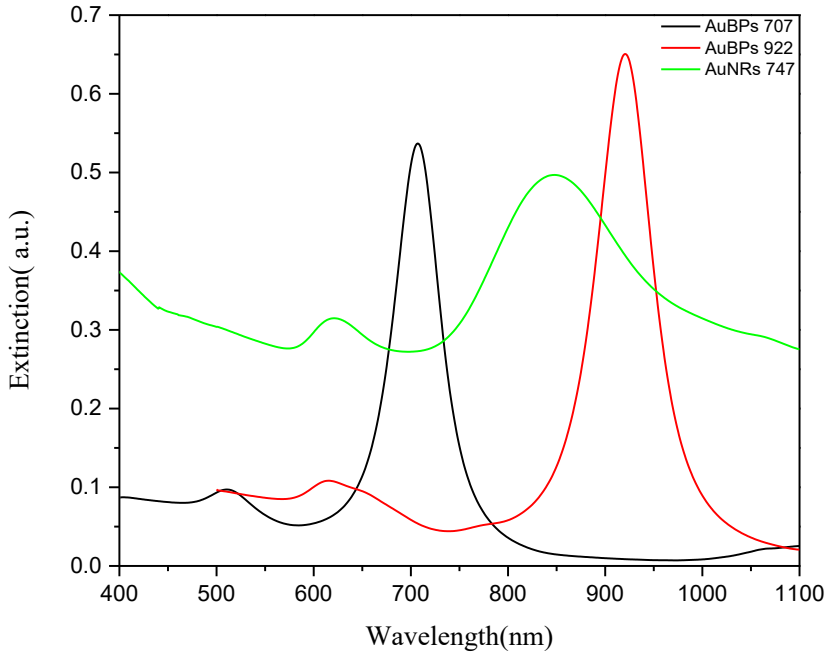

Figure 3.2 The extinction spectra of the gold nanoparticles deposited onto the PDMS substrate

3.2 Light Irradiation

For thermoplasmonic evaluation of the flexible plasmonic platforms, the substrates were positioned directly under the laser beam, with the lasers mounted 7 cm above the probe surface (Figure 3.3). Two laser wavelengths were employed: 532 nm and 685 nm. In the case of LED irradiation, the LEDs (532 nm, 660 nm, and 850 nm) were positioned at a distance of 1.3 cm from the probe and inclined at an angle between 15° and 30°, allowing the entire surface of the PDMS substrate coated with gold nanoparticles to be uniformly exposed while maintaining a clear field of view for the thermal imaging camera. Each light source (laser or LED) was applied independently for a duration of 15 to 20 minutes. Thermal images were captured at 30-second intervals throughout the irradiation period using an infrared thermal camera (Optirs PI Infrared Camera) capable of detecting temperature distributions across the sample surface.

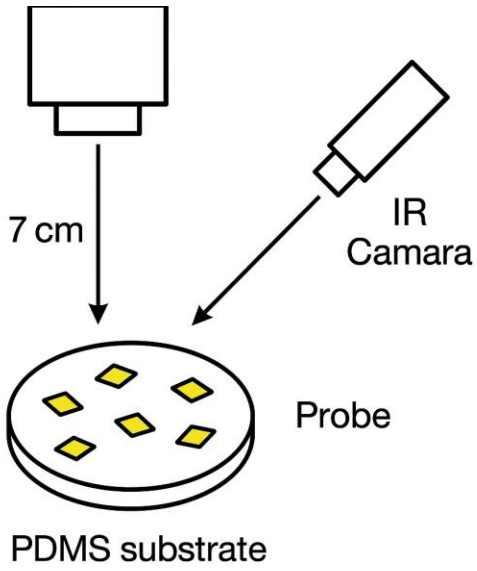

Figure 3.3 Schematic of the experimental setup used in this chapter

The starting temperature was typically 24 °C. The maximum temperatures reached by each substrate under each irradiation method are shown in Figure 3.4. As previously mentioned, I prepared six flexible plasmonic substrates using three types of nanoparticles: AuBPs with an LSPR peak at 707 nm, AuBPs with an LSPR peak at 921 nm, and AuNRs with an LSPR peak at 747 nm. Each nanoparticle type was deposited onto substrates that had been previously functionalized with either 3% or 5% APTES. In most cases, an increase in the APTES concentration led to higher temperatures during the irradiation. The most significant temperature increase due to a higher APTES concentration was observed for AuBPs921 irradiated with the 660 nm LED, where the temperature difference reached 4 °C (see Figure 3.4).

To better understand the photothermal effect on each substrate, a graph showing the temperature difference as a function of time was created for each laser/LED (Figures 3.5 to 3.9). In the case of the 532 nm laser (Figure 3.5), the targeted peak was the transverse one at approximately 520–530 nm. This peak is of low intensity, resulting in a smaller temperature increase during irradiation compared to the other wavelengths used. In this case, the highest temperature increase was observed for AuBPs707, with a ΔT of 3.7 °C. For the 685 nm laser (Figure3.6), the best-performing substrate was also AuBPs707, showing a temperature difference of 5.3 °C. With the 532 nm LED (figure 3.7), the temperature differences were around 2 °C, making it difficult to draw clear conclusions about which substrate performed better. The strongest photothermal response was observed with the 660 nm LED (Figure 3.8), where temperature differences ranged from 6 °C to 14 °C. The most significant increase was recorded for AuBPs921. Finally, for the 850 nm LED (Figure 3.9), the temperature differences ranged from approximately 4 °C to a maximum of 6.5 °C, the highest value being recorded for AuNRs747.

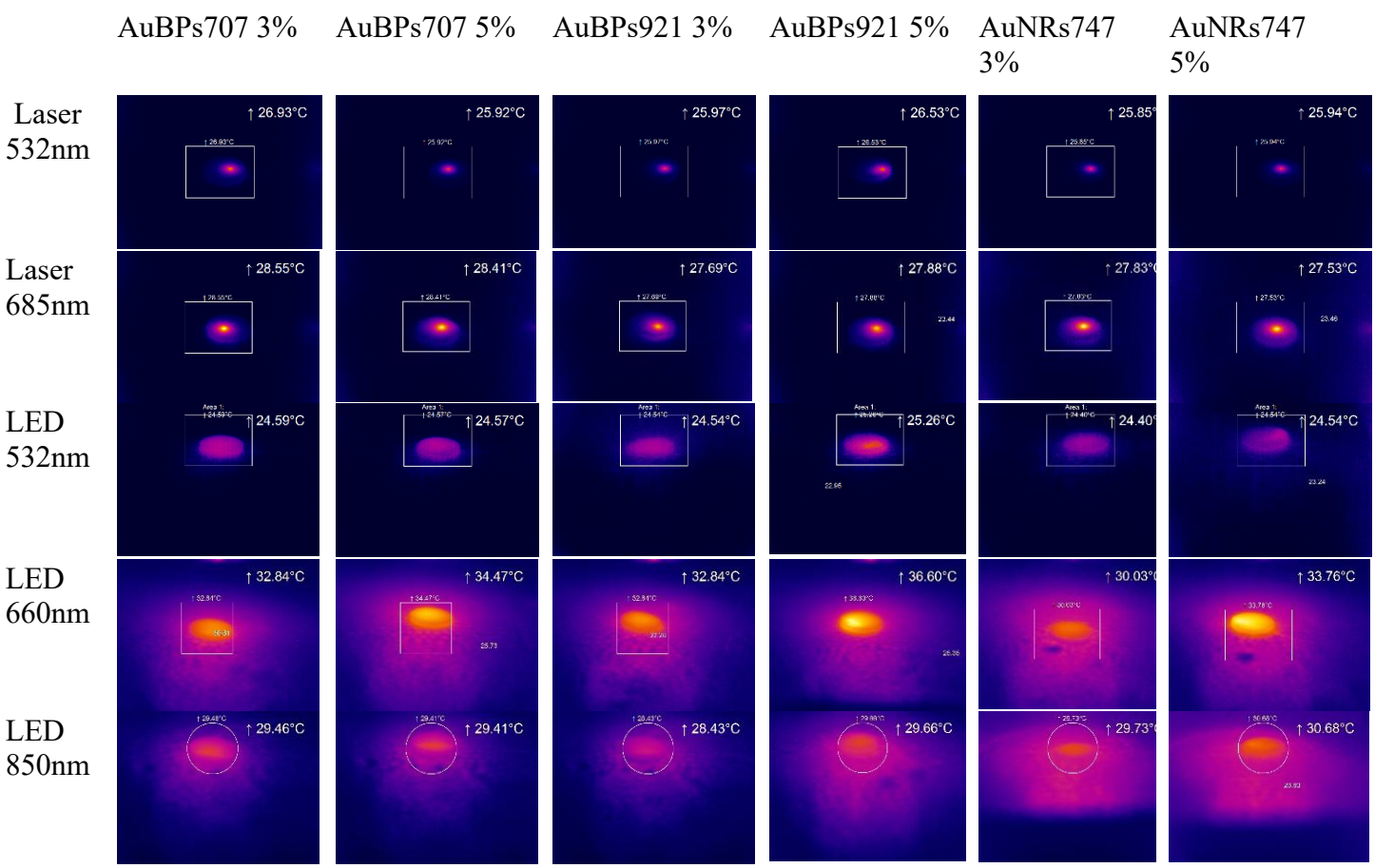

Figure 3.4 The thermic images recorded at the end of the 20 minutes irradiation of each sample

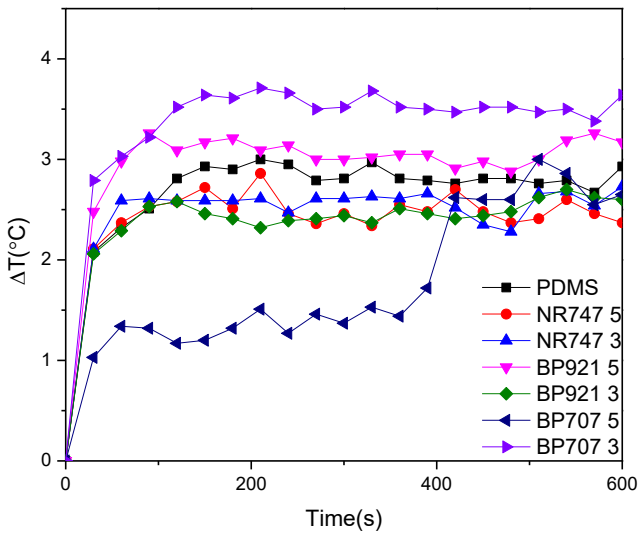

Figure 3.5 Difference of temperature in time after 10 minutes irradiation with laser 532nm

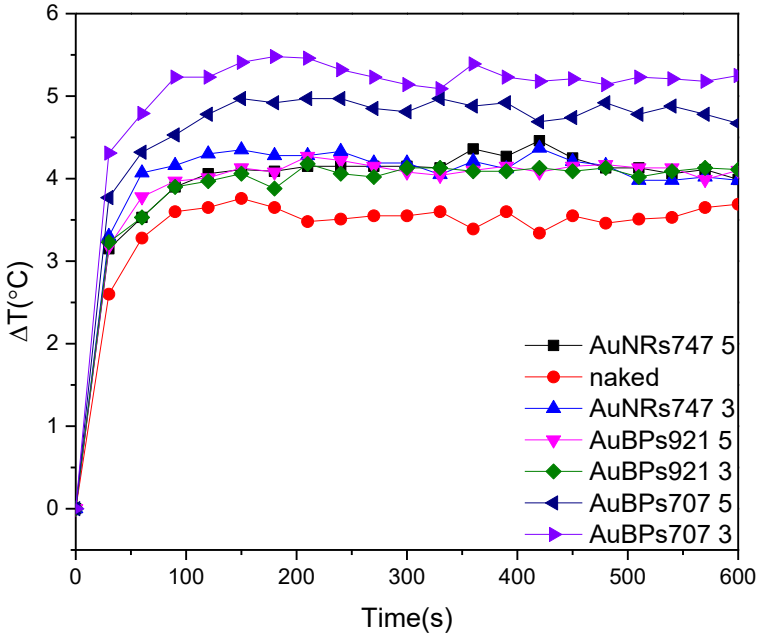

Figure 3.6 Difference of temperature in time after 10 minutes irradiation with laser 685nm

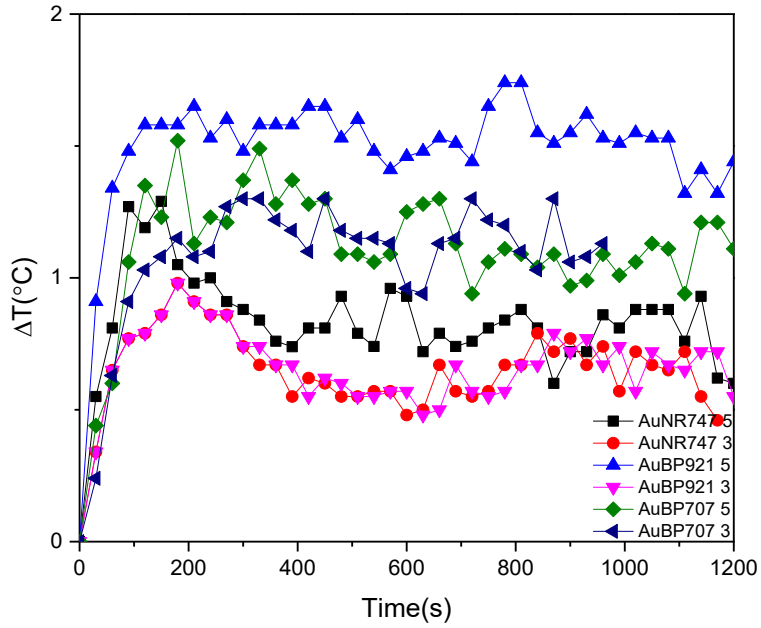

Figure 3.7 Difference of temperature in time after 20 minutes irradiation with LED 530nm

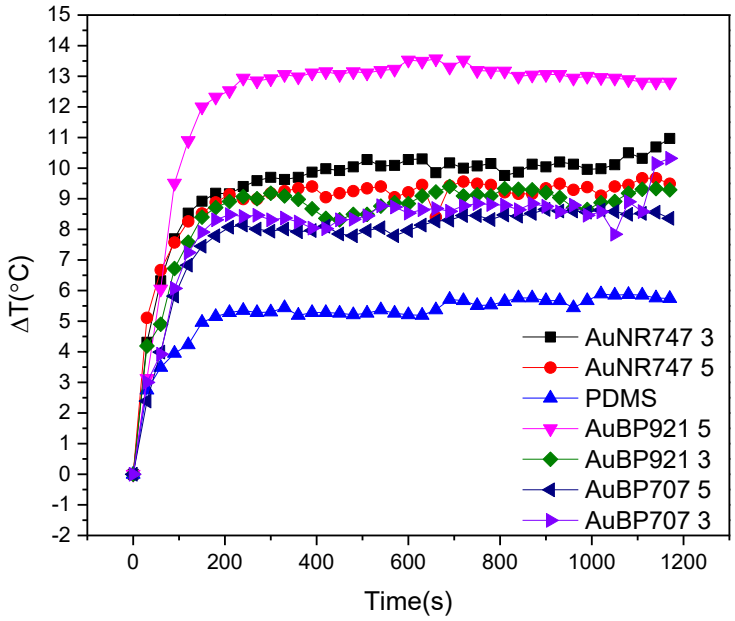

Figure 3.8 Difference of temperature in time after 20 minutes irradiation with LED 660nm

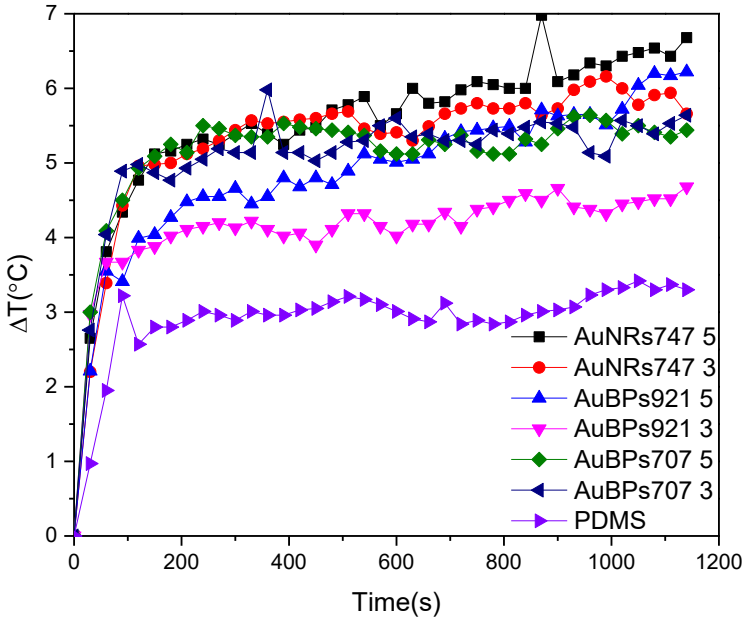

Figure 3.9 Difference of temperature in time after 20 minutes irradiation with LED 850nm

The photothermal experiments clearly demonstrate the importance of matching a nanoparticle's longitudinal plasmon resonance with the irradiation wavelength. For green light sources (532 nm laser and LED), the AuBPs707 samples exhibited the highest temperature increase—from 24 °C to 27 °C—due to better overlap with the excitation wavelength. Under red light (685 nm laser and 660 nm LED), the AuBPs921 (5%) samples showed superior performance, with temperatures rising from 24 °C to 36.6 °C. For near-infrared irradiation (850 nm LED), both AuNRs747 (5%) and AuBPs921 samples reached the highest temperatures, as their plasmon resonances are closest to this wavelength. In all cases, 5% APTES functionalization resulted in better nanoparticle attachment and enhanced photothermal effects compared to the 3% counterparts. These findings confirm that both precise plasmon tuning and effective surface functionalization are critical for maximizing photothermal efficiency in potential biomedical and sensing applications.

Conclusion and discussions

The present work focused on the synthesis, functionalization, and application of gold nanostructures—namely nanobipyramids and nanorods—both as plasmonic sensors and as photothermal agents. Throughout the study, careful control of synthesis parameters allowed the preparation of nanoparticles with well-defined geometries and tunable localized surface plasmon resonances (LSPR), which were further exploited in two complementary directions: detection of lead ions and photothermal heating under specific irradiation conditions.

In the sensing part, gold nanobipyramids immobilized on functionalized glass substrates demonstrated good sensitivity towards lead ions, detecting concentrations down to 2 μM. The sensing mechanism relied on the interaction between lead ions and nanoparticle surfaces, resulting in measurable shifts in the LSPR extinction spectra. The system proved to be robust and reproducible, suggesting its potential as a low-cost, rapid diagnostic tool for heavy metal detection in environmental or clinical samples.

In the photothermal studies, nanoparticle-coated flexible PDMS substrates were irradiated using multiple laser and LED sources. The results demonstrated that photothermal conversion efficiency depends strongly on the resonance match between the excitation source and the LSPR of the nanoparticles. AuBPs707 samples exhibited optimal heating under 532 nm irradiation; AuBPs921 performed best at 660–685 nm; AuBPs921 and AuNRs747 displayed superior heating under near-infrared (850 nm) excitation. Furthermore, increasing the functionalization degree from 3% to 5% consistently improved nanoparticle adhesion and overall heat generation.

Beyond these fundamental demonstrations, the potential applications of such plasmonic systems extend into emerging fields where controlled heating is desired. For instance, one promising avenue is the development of smart textiles or self-disinfecting surfaces. Embedding plasmonic nanoparticles into fabrics could allow garments to self-sterilize through photothermal heating, simply by exposure to sunlight or LED lamps, destroying pathogens without the need for chemical detergents. Similar approaches could be applied to hospital bed linens, air filtration membranes, or public transportation seats, reducing microbial contamination risks through non-invasive light-based activation. Additionally, plasmonic heating could find applications in anti-icing coatings, where controlled heating prevents ice formation on critical surfaces such as aircraft wings, wind turbines, or power lines.

In biomedical contexts, the demonstrated photothermal efficiency of the synthesized nanorods and bipyramids suggests their applicability in photothermal therapy (PTT) for localized tumor ablation, where heat is selectively generated in targeted tissues while minimizing collateral damage. Their tunable LSPR into the near-infrared region is particularly advantageous due to deeper tissue penetration of NIR light.

Overall, the versatility and multifunctionality of these gold nanostructures, together with their precise optical tunability and biocompatibility, position them as excellent candidates for next-generation

applications in sensing, medicine, materials science, and smart technologies. Future research may focus on improving large-scale fabrication, biocompatibility assessments, and device integration to bring these concepts closer to real-world implementations.

Appendix 1

The Jasco V-530 UV-Vis-IR spectrophotometer (Figure A1.1) is a device that measures the absorbance and transmittance of a colloidal sample. A representative diagram of the light path inside the instrument is shown in Figure A1.2. A beam of light is split into two beams with identical light intensities. One of the beams passes through a reference sample, while the other passes through the colloidal sample. Finally, the light intensities of the beams are detected after passing through the samples. Transmittance is defined as the ratio between the intensity of the beam passing through the colloid and the intensity of the beam passing through the reference sample.

$$Absorbance = log_{10}(Transmitance)$$

Figure A1.1 The spectrophotometer used for the absorbtion spectra spectra

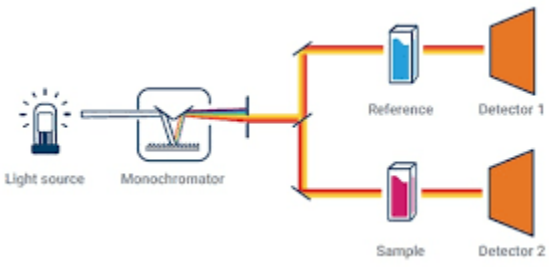

Figure A1.2 The light path inside the apparatus[26]

Appendix 2

The Hitachi SU3500 Scanning Electron Microscope (SEM; Figure A2.1) is a device that detects secondary electrons and other signals emitted from a sample after interaction with an electron beam. The microscope uses an electron source that produces a beam of electrons, which is focused onto the sample using various electromagnetic lenses. The sample generates three types of signals: secondary electrons, which provide information about surface topography; backscattered electrons, which give contrast based on atomic number; and X-rays, which offer information about elemental composition via EDX detectors. The working principle of the microscope is illustrated in Figure A2.2.

Figure A2.1 The SEM microscope used for recording the images in this paper

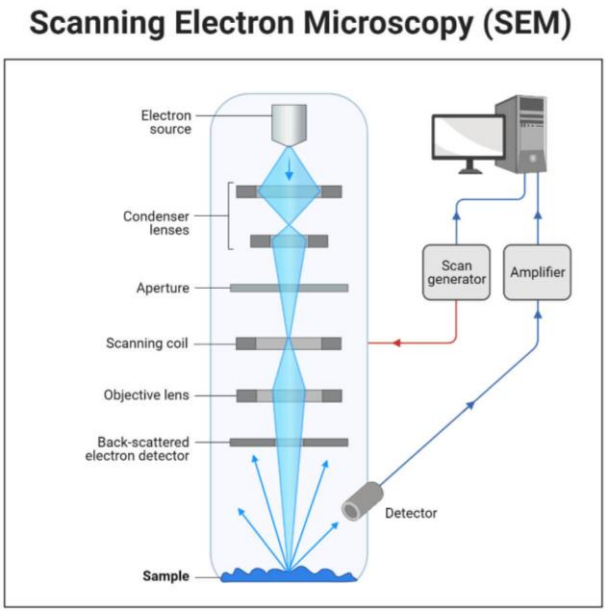

Figure A2.2 The working principle of a SEM[27]

References

[1] S. Hasan, "A Review on Nanoparticles: Their Synthesis and Types," vol. 4, 2015.

[2] C. Dumont *et al.*, "Solid lipid nanocarriers diffuse effectively through mucus and enter intestinal cells – but where is my peptide?," *Int. J. Pharm.*, vol. 586, p. 119581, Aug. 2020, doi: 10.1016/j.ijpharm.2020.119581.

[3] A. S. Pandey, D. Bawiskar, and V. Wagh, "Nanocosmetics and Skin Health: A Comprehensive Review of Nanomaterials in Cosmetic Formulations," *Cureus*, Jan. 2024, doi: 10.7759/cureus.52754.

[4] "Materials for electrochemical capacitors.pdf."

[5] M. A. Shah, B. M. Pirzada, G. Price, A. L. Shibiru, and A. Qurashi, "Applications of nanotechnology in smart textile industry: A critical review," *J. Adv. Res.*, vol. 38, pp. 55–75, May 2022, doi: 10.1016/j.jare.2022.01.008.

[6] Z. H. Mohammad, F. Ahmad, S. A. Ibrahim, and S. Zaidi, "Application of nanotechnology in different aspects of the food industry," *Discov. Food*, vol. 2, no. 1, Dec. 2022, doi: 10.1007/s44187-022-00013-9.

[7] S. A. Maier, *Plasmonics: Fundamentals and Applications*. New York, NY: Springer US, 2007. doi: 10.1007/0-387-37825-1.

[8] S.-Y. Lin, S.-W. Liu, C.-M. Lin, and C. Chen, "Recognition of Potassium Ion in Water by 15-Crown-5 Functionalized Gold Nanoparticles," *Anal. Chem.*, vol. 74, no. 2, pp. 330–335, Jan. 2002, doi: 10.1021/ac0156316.

[9] S.-Y. Lin, C. Chen, M.-C. Lin, and H.-F. Hsu, "A Cooperative Effect of Bifunctionalized Nanoparticles on Recognition: Sensing Alkali Ions by Crown and Carboxylate Moieties in Aqueous Media," *Anal. Chem.*, vol. 77, no. 15, pp. 4821–4828, Aug. 2005, doi: 10.1021/ac050443r.

[10] K. Saha, S. S. Agasti, C. Kim, X. Li, and V. M. Rotello, "Gold Nanoparticles in Chemical and Biological Sensing," *Chem. Rev.*, vol. 112, no. 5, pp. 2739–2779, May 2012, doi: 10.1021/cr2001178.

[11] T. L. Jennings, M. P. Singh, and G. F. Strouse, "Fluorescent Lifetime Quenching near $d = 1.5$ nm Gold Nanoparticles: Probing NSET Validity," *J. Am. Chem. Soc.*, vol. 128, no. 16, pp. 5462–5467, Apr. 2006, doi: 10.1021/ja0583665.

[12] C. Huang, Z. Yang, K. Lee, and H. Chang, "Synthesis of Highly Fluorescent Gold Nanoparticles for Sensing Mercury(II)," *Angew. Chem. Int. Ed.*, vol. 46, no. 36, pp. 6824–6828, Sep. 2007, doi: 10.1002/anie.200700803.

[13] K. Aslan, J. R. Lakowicz, and C. D. Geddes, "Nanogold Plasmon Resonance-Based Glucose Sensing. 2. Wavelength-Ratiometric Resonance Light Scattering," *Anal. Chem.*, vol. 77, no. 7, pp. 2007–2014, Apr. 2005, doi: 10.1021/ac0484880.

[14] R. Kurapova, L. Chouliaras, and J. T. O'Brien, "The promise of amplification assays for accurate early detection of α-synucleinopathies: A review," *Exp. Gerontol.*, vol. 165, p. 111842, Aug. 2022, doi: 10.1016/j.exger.2022.111842.

[15] H. Su, B. Sun, L. Chen, Z. Xu, and S. Ai, "Colorimetric sensing of dopamine based on the aggregation of gold nanoparticles induced by copper ions," *Anal. Methods*, vol. 4, no. 12, p. 3981, 2012, doi: 10.1039/c2ay25794g.

[16] J. H. Correia, J. A. Rodrigues, S. Pimenta, T. Dong, and Z. Yang, "Photodynamic Therapy Review: Principles, Photosensitizers, Applications, and Future Directions," *Pharmaceutics*, vol. 13, no. 9, p. 1332, Aug. 2021, doi: 10.3390/pharmaceutics13091332.
[17] Z. Dai, Ed., *Advances in Nanotheranostics I*, vol. 6. in Springer Series in Biomaterials Science and Engineering, vol. 6. Berlin, Heidelberg: Springer Berlin Heidelberg, 2016. doi: 10.1007/978-3-662-48544-6.
[18] N. N. M. Adnan *et al.*, "Effect of gold nanoparticle shapes for phototherapy and drug delivery," *Polym. Chem.*, vol. 7, no. 16, pp. 2888–2903, 2016, doi: 10.1039/C6PY00465B.
[19] D. Kim and H. Kim, "Numerical Study on Death of Squamous Cell Carcinoma Based on Various Shapes of Gold Nanoparticles Using Photothermal Therapy," *Sensors*, vol. 22, no. 4, p. 1671, Feb. 2022, doi: 10.3390/s22041671.
[20] H. Yue, L. Yuan, W. Zhang, S. Zhang, W. Wei, and G. Ma, "Macrophage responses to the physical burden of cell-sized particles," *J. Mater. Chem. B*, vol. 6, no. 3, pp. 393–400, 2018, doi: 10.1039/C7TB01673E.
[21] J. Domingo-Diez *et al.*, "Effectiveness of Gold Nanorods of Different Sizes in Photothermal Therapy to Eliminate Melanoma and Glioblastoma Cells," *Int. J. Mol. Sci.*, vol. 24, no. 17, p. 13306, Aug. 2023, doi: 10.3390/ijms241713306.
[22] D. Chateau *et al.*, "From gold nanobipyramids to nanojavelins for a precise tuning of the plasmon resonance to the infrared wavelengths: experimental and theoretical aspects," *Nanoscale*, vol. 7, no. 5, pp. 1934–1943, 2015, doi: 10.1039/C4NR06323F.
[23] D. Chateau, A. Desert, F. Lerouge, G. Landaburu, S. Santucci, and S. Parola, "Beyond the Concentration Limitation in the Synthesis of Nanobipyramids and Other Pentatwinned Gold Nanostructures," *ACS Appl. Mater. Interfaces*, vol. 11, no. 42, pp. 39068–39076, Oct. 2019, doi: 10.1021/acsami.9b12973.
[24] J.-M. Rye *et al.*, "Single gold bipyramids on a silanized substrate as robust plasmonic sensors for liquid environments," *Nanoscale*, vol. 10, no. 34, pp. 16094–16101, 2018, doi: 10.1039/C8NR03400A.
[25] Mehtala, J. G., Zemlyanov, D. Y., Max, J. P., Kadasala, N., Zhao, S., & Wei, A. (2014). Citrate-stabilized gold nanorods. *Langmuir*, *30*(46), 13727-13730.
[26] https://www.agilent.com/en/support/molecular-spectroscopy/uv-vis-uv-vis-nir-spectroscopy/uv-vis-spectroscopy-spectrophotometer-basics
[27] https://microbenotes.com/scanning-electron-microscope-sem/

DECLARAȚIE PE PROPRIE RĂSPUNDERE

Subsemnatul, Dincă Andrei Cristian, declar ca Lucrarea de disertație pe care o voi prezenta în cadrul examenului de finalizare a studiilor la Facultatea de Fizică, din cadrul Universității Babeș-Bolyai, în sesiunea Iulie 2025, sub îndrumarea, Conf. Dr. Monica Focșan, reprezintă o operă personală. Menționez că nu am plagiat o altă lucrare publicată, prezentată public sau un fișier postat pe internet. Pentru realizarea lucrării am folosit exclusive bibliografia prezentată și nu am ascuns o altă sursă bibliografică sau fișier electronic pe care să le fi folosit la redactarea lucrării.

Data 13.06.2025 Dincă Andrei Cristian,

Semnatura